2021

Nanomechanical and Chemical Mapping of the Structure and Interfacial Properties in Immiscible Ternary Polymer Systems

Hao-Xuan Lin

Thomas P. Russell

Dong Wang

Chinese Journal of
POLYMER SCIENCE 高分子科学

Nanomechanical and Chemical Mapping of the Structure and Interfacial Properties in Immiscible Ternary Polymer Systems

Li Hao-Xuan, Russell Thomas P., Wang Dong

Cite this article as:
Li Hao-Xuan, Russell Thomas P., Wang Dong. Nanomechanical and Chemical Mapping of the Structure and Interfacial Properties in Immiscible Ternary Polymer Systems[J]. *Chinese J. Polym. Sci*, In press. doi: 10.1007/s10118-021-2567-2

View online: https://doi.org/10.1007/s10118-021-2567-2

Chinese Journal of
POLYMER SCIENCE

RAPID COMMUNICATION

https://doi.org/10.1007/s10118-021-2567-2
Chinese J. Polym. Sci. **2021**, *39*, 651–658

Nanomechanical and Chemical Mapping of the Structure and Interfacial Properties in Immiscible Ternary Polymer Systems

Hao-Xuan Li[a], Thomas P. Russell[a,b,c], and Dong Wang[a*]

[a] *State Key Laboratory of Organic–Inorganic Composites & Beijing Advanced Innovation Center for Soft Matter Science and Engineering, Beijing University of Chemical Technology, Beijing 100029, China*
[b] *Polymer Science and Engineering Department, University of Massachusetts Amherst, Massachusetts 01003, United States*
[c] *Materials Sciences Division, Lawrence Berkeley National Laboratory, 1 Cyclotron Road, Berkeley, California 94720, United States*

Electronic Supplementary Information

Abstract It is a challenge to identify each phase in a multi-component polymer system and uniquely determine the interfacial properties between the different phases. Using atomic force microscopy nanomechanical mapping (AFM-NM) and AFM-based infrared spectroscopy (AFM-IR), we identify each phase, visualize structural developments, and determine the interfacial properties in a blend of three polymers: high-density polyethylene (HDPE), polyamide (PA6) and poly(styrene-*b*-ethylene-*co*-butylene-*b*-styrene) (SEBS). Each phase can be identified from the Young's modulus, along with the structural development within the phases before and after compatibilization. The interfacial widths between HDPE/PA6, HDPE/SEBS and SEBS/PA6 were determined independently in one measurement from a Young's modulus map. The structural, mechanical property development and identity of the phases were determined by AFM-NM, while AFM-IR, providing complementary chemical information, identified interfacial reactions, showed the chemical affinity of a compatibilizer with the component phases, and mapped the distribution of the compatibilizer in the ternary polymer blends. The chemical, structural and interfacial information obtained by these measurements provide information that is essential for producing mechanically robust materials from incompatible mixtures of polymers.

Keywords AFM nanomechanical mapping; AFM infrared spectroscopy; Multi-component systems; Interfacial structure; Interfacial properties

Citation: Li, H. X.; Russell, T. P.; Wang, D. Nanomechanical and chemical mapping of the structure and interfacial properties in immiscible ternary polymer systems. *Chinese J. Polym. Sci.* **2021**, *39*, 651–658.

INTRODUCTION

The interfacial properties between dissimilar polymers, including intermixing, extent of entanglements, structure and dynamics, dictate adhesion strength and fracture toughness between dissimilar polymers and the global mechanical properties of the mixture or composite. These are ultimately related to the segmental interactions between the components and their statistical segments lengths. Various reciprocal- and real-space techniques have been developed to assess composition profiles and structural variations across interfaces.[1–12] Interdiffusion, interfacial reaction kinetics and interfacial segregation have been investigated from the segment to polymer chain to macroscopic length scales and have provided quantitative insights into compatibilization, adhesion and fracture. These studies have been restricted to either two-component or two-phase systems where there is only one interface. However, we are often confronted with systems that have more than two components with more than two interfaces, and the characteristics of each of these interfaces are critical to the overall performance of such multi-component materials. Quantitatively interrogating each interface with a single measurement, which is critical for systems far removed from equilibrium, is difficult, if not impossible, in a single measurement.

Electron density contrast between different polymers can be small, making a unique identification of each phase difficult by electron microscopies. Double-staining[13] or selective etching[14,15] can be used to enhance contrast, at the risk of perturbing the virgin materials. Atomic force microscopy (AFM) phase imaging can be used to qualitatively distinguish different components.[16–18] However, since the phase image results from combined contributions of viscoelasticity, surface adhesion, and capillary forces of the material, it is difficult to extract quantitative information[19–21] and in some cases, depending on the set-point, phase images may lead to erroneous conclusions.[21] In some limited cases, spectroscopic imaging, for example tip-enhanced Raman spectroscopy, can be used to unravel chemical maps of analyzed materials.[22–27]

This shortfall in methods to characterize interfaces in multi-phase polymer systems becomes increasingly acute with not

* Corresponding author, E-mail: dwang@mail.buct.edu.cn
Received November 22, 2020; Accepted February 11, 2021; Published online March 16, 2021

only the desire to develop high-performance materials arising from synergistic interactions, but also the ever-increasing economic and environmental drive for the re-use of polymers where, for polymer upcycling, the mixing of polymers to produce a higher-valued end-product is of central interest.[14,15,28–30] However, since the blends of multi-phase polymers are generally thermodynamically immiscible, it is necessary to compatibilize these polymers to obtain useful mechanical and physical properties. Then, the use of a multi-phase compatibilizer to limit the size scale of the phase separated morphology and to promote adhesion between the different phases, become a convenient, low-cost and low-energy strategy to produce high-performance polymeric materials and to recycle polymeric materials to higher-valued materials. Up to now, the use of multi-phase compatibilizers has been engineering in nature with little, if any, fundamental understanding of the segregation of the compatibilizer at the different interfaces or the manner in which such compatibilizers modify the interfaces.[14,15,28–30]

AFM nanomechanical mapping (AFM-NM) has been shown to be a straightforward and simple means to investigate the interfaces between polymer systems where there are only two components or two phases.[31–38] AFM-based infrared spectroscopy (AFM-IR) is an emerging technique for chemical analysis and compositional mapping with spatial resolution of a few tens of nm.[39–50] Here, we used AFM-NM and AFM-IR to probe the effects of a multi-phase compatibilizer, comprised of graft copolymers of maleic anhydride (MAH) and styrene (St) melt-grafted onto HDPE (HDPE-*g*-MAH-*co*-St), on the structure and interfacial properties of a ternary polymer blend of high-density polyethylene (HDPE)/polyamide (PA6)/styrene-ethylene-butadiene-styrene (SEBS). The difference in the Young's moduli of the components enables the simultaneous mapping of structural development in the blends and a determination of the interfacial properties between the components. AFM-IR provides chemical variations across the interface, the spatial distribution of the compatibilizer in the blends, reactions occurring at the interface, and the chemical affinity of the compatibilizer with the components comprising the different phases. By combining AFM-NM and AFM-IR, the structural and mechanical property development, the spatial distribution of the compatibilizer in the three-component system, and the impact on the interfacial properties were elucidated.

EXPERIMENTAL

Materials

The high-density polyethylene (HDPE), polyamide (PA6), and styrene-ethylene-butadiene-styrene (SEBS) used are commercialized product. The HDPE (M572, M_w=1.36×10^5, MFR=2.2 g/10min at 190 °C/2.16kg), PA6 (1013B, M_w=2.3×10^4, MFR=15.8 g/10min at 230 °C/2.16kg), and SEBS (G1652, styrene content: 29 wt%, M_w=1.35×10^5, MFR=4.9 g/10min at 230 °C/5.0kg) were supplied by Yanshan Petrochemical Co., Ube Co., and KRATON, respectively. Maleic anhydride (MAH) (99%), styrene monomer (St) (≥99%), and dicumyl peroxide (DCP) (98%) were obtained from Sigma-Aldrich and used without further purification.

MAH-St melt grafted HDPE (HDPE-*g*-MAH-*co*-St), the multi-phase compatibilizer, was prepared and characterized following the procedures given in the literature.[14,51] The grafting reactions were conducted in a Rheocord Haake batch mixer with 50 cm^3 chamber. The MAH, liquid styrene monomer and peroxide were first mixed and then the mixture was pre-mixed with HDPE. The resulting mixture was charged into the chamber and mixed at 180 °C for 10 min. The resultants were then dissolved in boiled xylene and then precipitated using excess of acetone. The absorption peaks at 1785 and 1090 cm^{-1} in the FTIR spectra (Fig. S1 in the electronic supplementary information, ESI) of the purified HDPE-*g*-(MAH-*co*-St) confirmed the presence of MAH and St groups grafted onto the HDPE. The grafting content of MAH and St of the as-prepared samples are 0.98 wt% and 1.25 wt%, respectively.

Sample Preparation

All compositions used for blending were dried in a vacuum oven at 80 °C for 10 h and used immediately. The ternary blends of HDPE/PA6/SEBS without and with the compatibilizer were prepared using melt-blending at 230 °C in the same mixer. The rotation speed was set at 60 r/min and the mixing time was 8 min. The formulation of blends with 5 wt% compatibilizer is (HDPE+HDPE-*g*-(MAH-*co*-St))/PA6/SEBS ((65+5)/15/15). The amount of HDPE and compatibilizer in other blends were adjusted accordingly. The resulting blends were ultramicrotomed at −150 °C using a cryo-ultramicrotome (Leica EM FC7) with a diamond knife to remove the top surface of the blends, leaving a smooth surface for AFM-NM and AFM-IR measurements. The as-prepared samples have a surface roughness R_q of 9.8±0.6 nm over a 15 μm × 15 μm scanning area. For mechanical testing samples, the as-prepared blends were hot-pressed at 15 MPa and 230 °C to obtain the composite sheets with a thickness of 1 mm.

AFM Nanomechanical Mapping (AFM-NM) Characterizations

AFM-NM was carried out on a Bruker MultiMode 8 AFM using PeakForce QNM mode. OMCL-AC160TS-R3 cantilevers (OLYMPUS Micro Cantilevers) were used for scanning, during which the oscillation frequency of the Z-piezo and force amplitude was set at 1.0 kHz and 150 nm, respectively, and a scan rate of 0.5 Hz was used. The actual spring constant of the cantilevers was measured using a thermal tune method. A tip-check sample (Aurora Nanodevices, Canada) was used to estimate the tip geometry using tapping mode imaging. The scan area and scan rate were 2.0 μm × 2.0 μm and 1 Hz, respectively. The details of QNM mode were provided in the Supporting Information.

AFM-IR Characterizations

AFM-IR was performed on a Bruker nanoIR3 using contact mode. The samples were scanned using PR-EX-nIR2-10 tips to acquire the topography. Then, the samples were illuminated from the top of the side with Bruker Hyperspectral QCL laser across the 800–1900 cm^{-1} at a spectral resolution of 2 cm^{-1}. For AFM-IR images, the AFM tip scans across the sample surface, during which the sample is illuminating at a desired wavelength. For AFM-IR spectra, the resonance enhanced thermal expansion of the sample is measured as a function of the laser wavelength with the AFM tip. The laser wavelength is normalized by the laser intensity averaged over 128 pulses.

https://doi.org/10.1007/s10118-021-2567-2

Detailed principles of the AFM-IR can be found in the reported studies.[39–41]

FTIR Measurements

FTIR measurements were performed on a Nicolet 6700 spectrometer using ATR mode. The instrument was operated in the range of 800–1900 cm^{-1} at the resolution of 2 cm^{-1}. The spectra were an average of 64 scans.

Tensile Testing

Tensile testing was carried out on an Instron 3345 tensile tester at a strain rate of 50 mm/min at room temperature. The tensile bar is dog-bone-shape with dimensions of 50 (length) mm × 4 mm (width) × 1.0 mm (thickness).

RESULTS AND DISCUSSION

Table 1 and Fig. 1 show the mechanical properties of the HDPE/PA6/SEBS ternary blends with and without the multi-phase compatibilizer. The results show that by increasing the content of HDPE-*g*-(MAH-*co*-St), both the elongation and stress at break increase greatly. With 15 wt% compatibilizer, the elongation and stress at break of the compatibilized blends were 6.8 and 1.6 times higher than those of the uncompatibilized blends, respectively, while the yield stresses were almost unchanged (Table 1 and Fig. 1), demonstrating the efficiency of the HDPE-*g*-(MAH-*co*-St) in improving the compatibilization of various polymer pairs and, therefore, in promoting the toughness of the ternary blends.[14,15]

Table 1 Mechanical properties of the HDPE/PA6/SEBS ternary blends with the multi-phase compatibilizer loading.

Blends	Yield stress (MPa)	Stress at break (MPa)	Elongation at break (%)
0 wt%	19.3±0.8	13.1±0.2	106.1±26.6
5 wt%	19.5±0.3	15.2±0.3	226.7±45.6
10 wt%	22.8±2.7	16.0±1.2	353.4±23.4
15 wt%	21.2±0.9	21.0±0.5	717.7±56.6

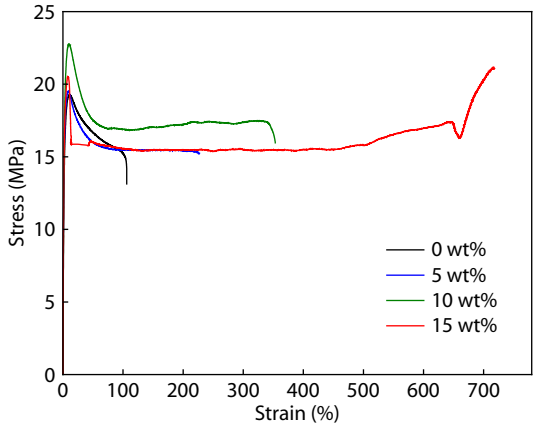

Fig. 1 The stress-strain curves of the HDPE/PA6/SEBS (70/15/15) blends without and with HDPE-*g*-(MAH-*co*-St) multi-phase compatibilizer.

Fig. 2 and Fig. S2 (in ESI) show AFM-NM results of the uncompatibilized and compatibilized HDPE/PA6/SEBS blends. With only height images (Figs. 2a and 2b), the individual component in the ternary blends is unidentifiable, while with the Young's modulus maps (Figs. 2a' and 2b'), the identification of each component becomes easy. The bright regions with higher Young's modulus are assigned to the PA6 dispersed phase, the dark regions with lower modulus are assigned to the SEBS, and the light brown regions with an intermediate modulus are assigned to the HDPE matrix. A Young's modulus profile in Fig. 2(c) clearly shows the modulus difference of the HDPE, PA6 and SEBS components. The histogram in Fig. 2(d) shows the statistical results of Young's modulus of the uncompatibilized blends where a Gaussian function fitting gives a mean value of 1.60 (1.42–1.75) GPa for HDPE and 2.27 (2.18–2.42) GPa for PA6, and a Lorentz function fitting gives a mean value of 158 (143–169) MPa for SEBS. These measured Young's moduli of the HDPE and PA6 are consistent with the bulk values, while for the SEBS, it is much higher than the bulk value. This can arise from the large deformation resulting from the tapping force and high oscillation frequency of the Z-piezo that is applied to SEBS elastomer. The measured Young's moduli of the HDPE, PA6 and SEBS are sufficient to identify the compositions in those blends.

With the assignment of the three components, the modulus map in Fig. 2(a) shows large discrete domains of PA6 and SEBS dispersed in an HDPE matrix. Most PA6 domains are several microns in size and a few are several hundred nanometers in size, that are entirely or partially encapsulated by SEBS, forming a rigid core-rubber like shell structure in HDPE matrix. With the introduction of the multi-phase compatibilizer, it is evident that the sizes of the dispersed domains decreased and the size distributions narrowed. The number of the core-shell structures significantly increased with the use of the compatibilizer. Three different mechanisms give rise to these morphological changes. First, for the immiscible HDPE and PA6 pair, the MAH groups in HDPE-*g*-(MAH-*co*-St) will react or have an affinity with the amine groups in PA6, markedly enhancing the adhesion between the HDPE and PA6, which is a well-known compatibilization strategy. Second, for the partially miscible HDPE and SEBS pair, the styrene groups in HDPE-*g*-(MAH-*co*-St) interact favorably with SEBS, which increases the adhesion between the HDPE and SEBS. Third, for the immiscible PA6 and SEBS pair, reactions between the MAH groups in HDPE-*g*-(MAH-*co*-St) and amines groups in PA6 lead to the formation of graft copolymers of HDPE-*g*-(MAH-*co*-St) and PA6 while, the styrene groups, promote interactions between the PA6 and SEBS. The detailed compatibilization will be discussed below from the results of AFM-NM and AFM-IR, respectively. Consequently, this multi-phase compatibilizer will reduce the interfacial tension of all the interfaces and promote adhesion between the different phases.[14,15,52,53]

Fig. 3 shows the Young's modulus maps of the blends with scans across the interfaces. For the uncompatibilized blends, the HDPE/PA6, HDPE/SEBS and SEBS/PA6 interfaces are smooth, minimizing the interfacial area between the components. With introduction of the HDPE-*g*-(MAH-*co*-St), the interfaces become very rough. Line scans across different interfaces were used to determine the change in the Young's modulus across the HDPE/SEBS, SEBS/PA6 and HDPE/PA6 interfaces and the interfacial width can be estimated from a hyperbolic tangent function fit to the modulus profiles (Fig. 4).

https://doi.org/10.1007/s10118-021-2567-2

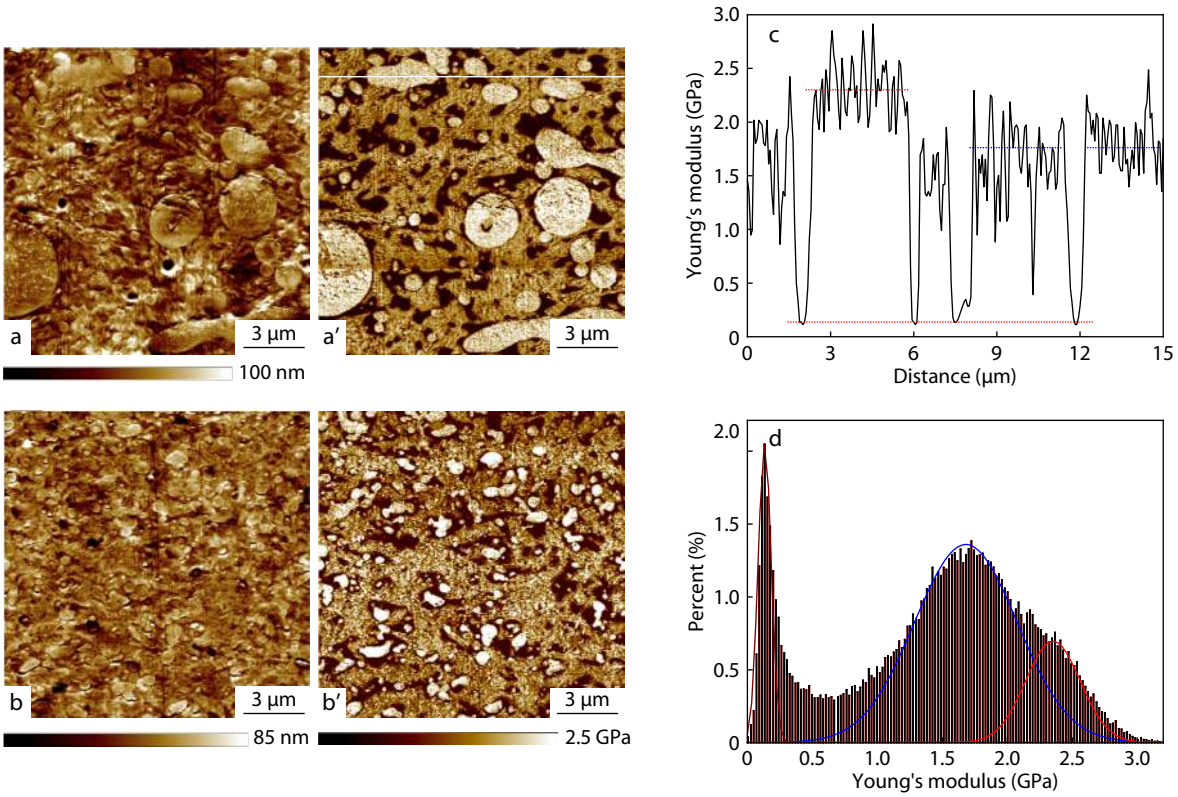

Fig. 2 AFM-NM results of the uncompatibilized and compatibilized HDPE/PA6/SEBS blends with 15 wt% compatibilizer. (a, b) Height images and (a', b') corresponding Young's modulus maps of the uncompatibilized and compatibilized blends. (c) Young's modulus profile of line scan in (a') across the HDPE, PA6 and SEBS domains. A line scan across the HDPE, PA6 and SEBS domains in compatibilized blends in (b') shown in Fig. S3 (in ESI). (d) Young's modulus distribution of the uncompatibilized blends. The dashed and solid red, blue and brown lines in (c) and (d) are indication of the Young's modulus and function fitting of the PA6, HDPE, and SEBS components.

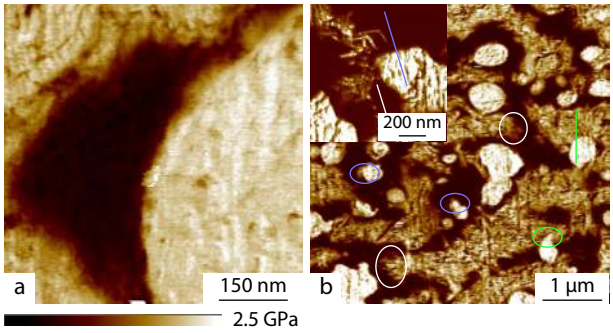

Fig. 3 Young's modulus maps of the uncompatibilized (a) and compatibilized (b) HDPE/PA6/SEBS blends at the interfacial regions. The white, light blue and green ellipses in (b) indicate the interfacial roughening between the HDPE/SEBS, PA6/SEBS and HDPE/PA6.

The interfacial widths between HDPE/SEBS, SEBS/PA6 and HDPE/PA6 in the uncompatibilized blends are small, in the range of 8–12 nm in size (Fig. 4a and Fig. S4 in ESI). After compatibilization, it increases to 35.0±5.6 nm for HDPE/SEBS, 32.9±4.8 nm for SEBS/PA6, and 40.0±5.8 nm for HDPE/PA6 (the interfacial widths between various pairs are listed in Table 2). Previous information on interfacial width between a reactive compatibilized HDPE/PA6 pair and polymer pairs compatibilized by chemical affinity (HDPE/SEBS and SEBS/PA6), prepared by melt blending, are not available. The interfacial width is usually measured in a thermally annealed bilayer geometry. For example, Inoue *et al.* reported that, for the reactive polypropylene (PP-*g*-MAH)/PA6 bilayer system, the interfacial width increased to ~40 nm after annealing, while it was a constant value at ~5 nm for non-reactive system.[54] For a polymer pair compatibilized by chemical affinity, as reported by Russell *et al.*, the interfacial width between polystyrene (PS)/poly(methyl methacrylate) (PMMA) increased from 5 nm to 30 nm after compatibilization using a copolymer of PS-*b*-MMA.[3] Although the reported interfacial width here cannot be used to make direct comparisons with X-ray or neutron reflectivity results, since the sample preparation conditions are markedly different, the broadening of all the interfaces due to the presence of the HDPE-*g*-(MAH-*co*-St) is apparent. It should also be noted that, for semi-crystalline HDPE and PA6, the measured interfacial width cannot be taken as absolute, since the orientation of the crystals can influence the width of the interface measured. Other factors, like surface roughness may also induce an error to the measured interfacial width. However, since the results represent an average over 20 single modulus profiles, the influence of the morphology, when comparing the mixtures with and without the compatibilizer, should not be compromised.

Fig. 5 and Fig. S5 (in ESI) show the AFM-IR maps of the uncompatibilized and compatibilized HDPE/PA6/SEBS band at 1785 cm^{-1}. The band at 1785 cm^{-1} is a characteristic absorp-

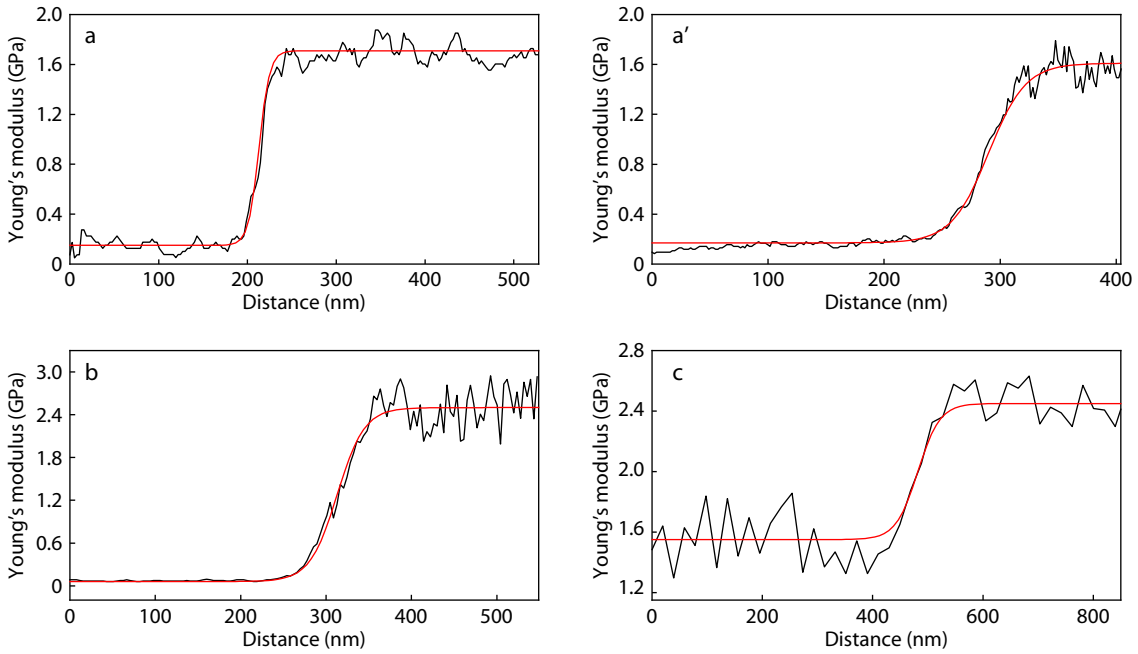

Fig. 4 Young's modulus profiles across the interfacial regions between the HDPE/SEBS in uncompatibilized (a) and compatibilized (a') HDPE/PA6/SEBS blends. (b, c) Profiles across the SEBS/PA6 and HDPE/PA6 interfacial regions in compatibilized blends.

Table 2 Interfacial widths determined by AFM-NM between the three polymer pairs at different compatibilizer loadings.

Sample	Interfacial width (nm)			
	0 wt%	5 wt%	10 wt%	15 wt%
HDPE/SEBS	8.8±2.6	24.0±3.8	32.4±5.1	35.0±5.6
SEBS/PA6	8.4±2.3	21.6±3.7	29.6±4.2	32.9±4.8
HDPE/PA6	12.2±3.4	28.8±5.1	36.3±6.0	40.0±5.8

tion of symmetric C=O stretching of the anhydride group, enabling a mapping of the distribution of HDPE-*g*-(MAH-*co*-St) in the ternary blends. The absorption peak of the styrene can also be used to map the distribution, since the system contains SEBS, so the absorption of the anhydride groups was used. As seen in Figs. 5(a) and 5(b), the AFM-IR images show a phase-separated morphology that is consistent with the AFM-NM results. The bright-yellow regions with higher AFM-IR signal are assigned to the PA6 dispersed phase, the dark regions with lower signal are assigned to the SEBS, and the orange regions with an intermediate signal are assigned to the HDPE. The identification of the HDPE, SEBS and PA6 in the AFM-IR images were confirmed by comparison of the FTIR and AFM-IR spectra (Figs. S6 and S7 in ESI). For uncompatibilized blends, PA6 has a strong absorption band at 1632 cm^{-1} (Fig. S7 in ESI), characteristic of C=O stretching and HDPE has a strong absorption at 1472 cm^{-1}, arising from CH_2 bending. SEBS has an absorption characteristic of CH_2 bending at 1454 cm^{-1}, but it is weak. Therefore, when imaging at 1785 cm^{-1}, PA6 has the highest AFM-IR signal, HDPE has an intermediate value and SEBS shows the lowest signal.

Fig. 5(c) and Fig. S8 (in ESI) show the AFM-IR spectra acquired in the SEBS/PA6, HDPE/SEBS, and HDPE/PA6 interfacial regions. For thin film samples, the film thickness can affect the measured IR intensity, which is absent for the bulk samples used in the current studies. Therefore, the intensity of the AFM-IR signal reflects the concentrations of the anhydride groups in the imaged areas. Fig. 5(d) shows the normalized value of the ratio of the band area of the characteristic absorption of the anhydride groups from 1768 cm^{-1} to 1820 cm^{-1} at 5 wt%, 10 wt% and 15 wt% compatibilizer loadings to that of without the compatibilizer, acquired at different interfacial regions. At the SEBS/PA6 interface, with increasing compatibilizer loading, the concentration of the anhydride increases, while at the HDPE/PA6 interface, the increase is much more marked. Consequently, the anhydride groups are enriched at the HDPE/PA6 interface, due to the strong chemical affinity between the anhydride groups in the compatibilizer and amine groups in PA6. It should be noted that only very limited number of anhydrides groups reacted with the amine groups in PA, as evidenced in Fig. 6, where only trace amounts of carbonyl imide linkages between the anhydride groups in the compatibilizer and amine groups in PA6 are observed. In fact, even for a model bilayer sample consisting of amine-terminal polystyrene (PS-NH_2) and anhydride-terminal poly(methyl methacrylate) (PMMA-anh), both having molecular weight lower than 3×10^4 (M_n) and annealed for many hours, the conversion of PS-NH_2 (or PMMA-anh) into PS-*b*-PMMA copolymer is limited,[5,55,56] only several percent in some cases.[55] Considering the much higher molecular weights of the components (all three polymers are commercial products), the mechanical blending conditions (as opposed to the simple annealing of model bilayer sample), and the complexity of the ternary blends, the number of anhydrides reacted is negligible.

In the compatibilized blends, a small absorption band at 1722 cm^{-1} appears at higher compatibilizer loading (Fig. 6), corresponding to an absorption of the carbonyl imide link-

https://doi.org/10.1007/s10118-021-2567-2

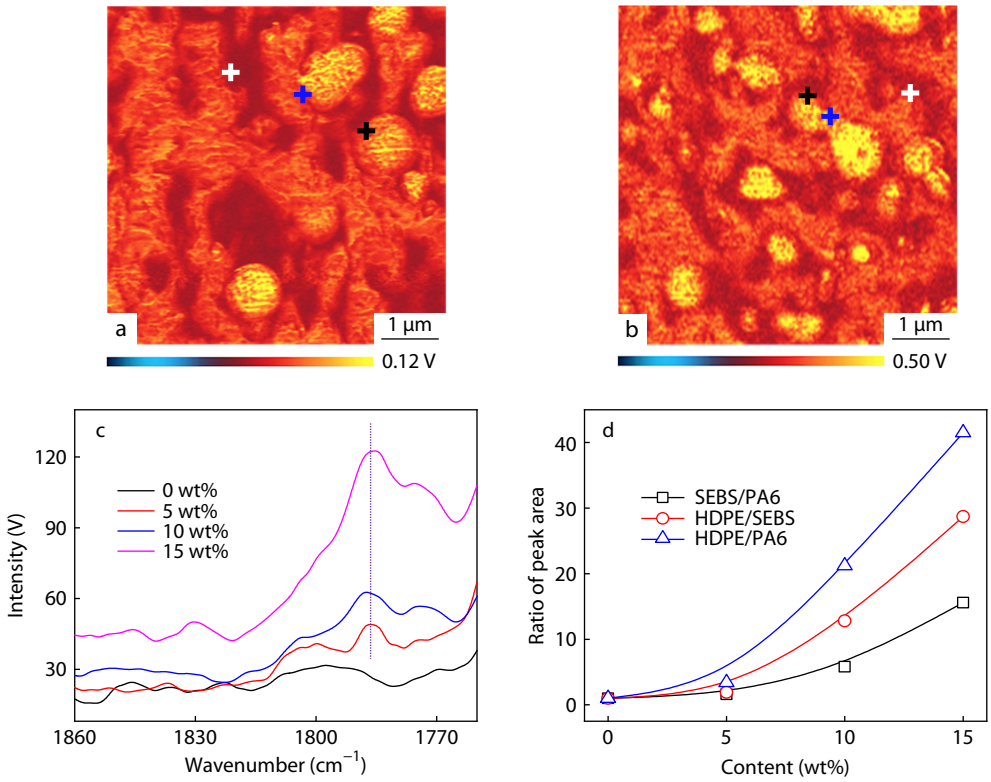

Fig. 5 AFM-IR maps of the uncompatibilized (a) and compatibilized (b) HDPE/PA6/SEBS blends with 15 wt% compatibilizer. AFM-IR spectra acquired at the (c) HDPE/SEBS interfacial regions, indicated by the white crosses in (a, b). (d) Normalized ratios of the band at 1785 cm^{-1} acquired at the SEBS/PA6, HDPE/SEBS and HDPE/PA6 interfaces.

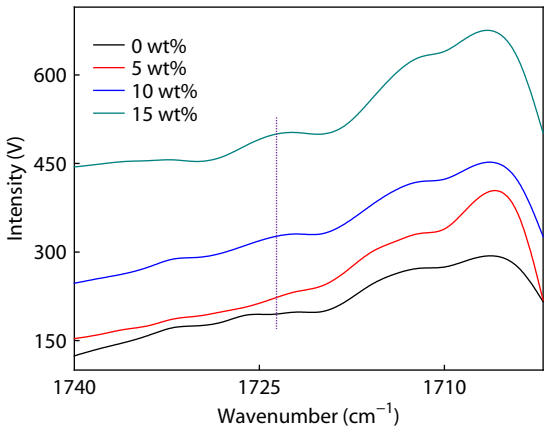

Fig. 6 AFM-IR spectra acquired at the HDPE/PA6 interfacial regions where a small imide band appears.

age between the anhydride groups in the compatibilizer and amine groups in PA6, a strong indication of a reactive compatibilization.[57,58] It should be noted that, even with the formation of the imide linkages, a clear shift of the C=O stretching of anhydride group at 1785 cm^{-1} to a lower wavenumber is not observed. However, given the very low fraction of reacted anhydride groups, the absence of this shift is not surprising.

From the AFM-NM and AFM-IR results, it is evident that the markedly broadened interfacial width due to a simple reduction in the interfacial energy by the compatibilizer, interfacial reactions of the compatibilizer with components at the interface, and the chemical affinity of the compatibilizer with the component phases are readily discerned. The markedly increased interfacial width and the number of core-shell structures formed, where the rigid PA6 particles are encapsulated by the SEBS elastomer in HDPE matrix, as well as AFM-NM and AFM-IR reveals that such a synergy is crucial for the significantly increased toughness of the ternary polymer blends.

CONCLUSIONS

In summary, we have shown that nanomechanical and infrared chemical mapping of a HDPE/PA6/SEBS ternary blend can easily map the structure and interfacial properties in a multi-component polymer system, which were difficult to access previously. The morphology of the ternary blend, based on the Young's moduli of the constituents, allows direct identification of the component phases, insights into the development of all of the interfaces, and a mean to correlate changes of the interfaces with mechanical properties. The morphology observed by nanochemical mapping agrees well with that observed by nanomechanical mapping. Further, the spatial distribution of the compatibilizer at the various interfaces and within the domains was observed, uncovering interfacial reactions and preferential chemical affinity of the compatibilizer with the component phases. The AFM nanomechanical and chemical mapping show tremendous promise for the investigation of a wide range of

https://doi.org/10.1007/s10118-021-2567-2

structural changes and interfacial phenomena in a multi-component polymer system with complex multi-phased morphologies.

Electronic Supplementary Information

Electronic supplementary information (ESI) is available free of charge in the online version of this article at http://dx.doi.org/10.1007/s10118-021-2567-2.

ACKNOWLEDGMENTS

This work was financially supported by the National Natural Science Foundation of China (No. 51673016) and the Beijing Advanced Innovation Center for Soft matter Science and Engineering. The authors thank Dr. Dengli Qiu, Dr. Yaolun Liu at Bruker, and Prof. Toshio Nishi at Tokyo Institute of Technology for technical support and helpful discussions.

REFERENCES

1 Composto, R. J.; Kramer, E. J.; White, D. M. Mutual diffusion in the miscible polymer blend polystyrene/poly(xylenyl ether). *Macromolecules* **1988**, *21*, 2580–2588.
2 Schulze, J. S.; Cernohous, J. J.; Hirao, A.; Lodge, T. P.; Macosko, C. W. Reaction kinetics of end-functionalized chains at a polystyrene/poly(methyl methacrylate) interface. *Macromolecules* **2000**, *33*, 1191–1198.
3 Russell, T. P.; Menelle, A.; Hamilton, W. A.; Smith, G. S.; Satija, S. K.; Majkrzak, C. F. Width of homopolymer interfaces in the presence of symmetric diblock copolymers. *Macromolecules* **1991**, *24*, 5721–5726.
4 Perrin, P.; Prud'homme, R. E. SAXS measurements of interfacial thickness in amorphous polymer blends containing a diblock copolymer. *Macromolecules* **1994**, *27*, 1852–1860.
5 Zhang, J. B.; Lodge, T. P.; Macosko, C. W. Interfacial morphology development during PS/PMMA reactive coupling. *Macromolecules* **2005**, *38*, 6586–9651.
6 Charoensirisomboon, P.; Chiba, T.; Solomko, S. I.; Inoue, T.; Weber, M. Reactive blending of polysulfone with polyamide: a difference in interfacial behavior between *in situ* formed block and graft copolymers. *Polymer* **1999**, *40*, 6803–6810.
7 Pablo Tomba, J.; Carella, J. M.; Pastor, J. M. Molecular mechanisms of interphase evolution in the liquid polystyrene-glassy poly(phenylene oxide) system. *Macromolecules* **2009**, *42*, 3565–3572.
8 Sauer, B. B.; Walsh, D. J. Use of neutron reflection and spectroscopic ellipsometry for the study of the interface between miscible polymer films. *Macromolecules* **1991**, *24*, 5948–5955.
9 Liao, Y. G.; Nakagawa, A.; Horiuchi, S. Interdiffusion at homopolymer/random copolymer interfaces investigated by energy-filtering transmission electron microscopy. *Macromolecules* **2007**, *40*, 7966–7972.
10 Qiu, H.; Bousmina, M. Determination of mutual diffusion coefficients at nonsymmetric polymer/polymer interfaces from rheometry. *Macromolecules* **2000**, *33*, 6588–6594.
11 Higashida, N.; Kressler, J.; Yukioka, S.; Inoue, T. Ellipsometric measurements of positive η parameters between dissimilar polymers and their temperature dependence. *Macromolecules* **1992**, *25*, 5259–5262.
12 Iubek, G.; Pionteck, J.; Bondarenko, V.; Pompe, G.; Taesler, Ch.; Petters, K.; Krause-Rehberg, R. Positron annihilation lifetime spectroscopy (PALS) for interdiffusion studies in disperse blends of compatible polymers: a quantitative analysis. *Macromolecules* **2002**, *35*, 6313–6323.
13 Shimizu, H.; Li, Y. J.; Kaito, A.; Sano, H. Formation of nanostructured PVDF/PA11 blends using high-shear processing. *Macromolecules* **2005**, *38*, 7880–7883.
14 Wang, D.; Li, Y.; Xie, X. M.; Guo, B. H. Compatibilization and morphology development of immiscible ternary polymer blends. *Polymer* **2011**, *52*, 191–200.
15 Li, H. M.; Xie, X. M. Morphology development and superior mechanical properties of PP/PA6/SEBS ternary blends compatibilized by using a highly efficient multi-phase compatibilizer. *Polymer* **2017**, *108*, 1–10.
16 Garcia, R.; Magerle, R.; Perez, R. Nanoscale compositional mapping with gentle forces. *Nat. Mater.* **2007**, *6*, 405–411.
17 Cleveland, J. P.; Anczykowski, B.; Schmid, A. E.; Elings, V. B. Energy dissipation in tapping-mode atomic force microscopy. *Appl. Phys. Lett.* **1998**, *72*, 2613–2615.
18 Wang, D.; Russell, T. P. Advances in atomic force microscopy for probing polymer structure and properties. *Macromolecules* **2018**, *51*, 3–24.
19 Tamayo, J.; Garcia, R. Effects of elastic and inelastic interactions on phase contrast images in tapping-mode scanning force microscopy. *Appl. Phys. Lett.* **1997**, *71*, 2394–2396.
20 Garcia, R.; Gomez, C. J.; Martinez, N. F.; Patil, S.; Dietz, C.; Magerle, R. Identification of nanoscale dissipation processes by dynamic atomic force microscopy. *Phys. Rev. Lett.* **2006**, *97*, 016103.
21 Knoll, A.; Magerle, R.; Krausch, G. Tapping mode atomic force microscopy on polymers: where is the true sample surface? *Macromolecules* **2001**, *34*, 4159–4165.
22 Verma, P. Tip-enhanced Raman spectroscopy: technique and recent advances. *Chem. Rev.* **2017**, *117*, 6447–6466.
23 Xue, L. J.; Li, W. Z.; Hoffmann, G. G.; Goossens, J. G. P.; Loos, J.; de With, G. High-resolution chemical identification of polymer blend thin films using tip-enhanced Raman mapping. *Macromolecules* **2011**, *44*, 2852–2858.
24 Yeo, B. S.; Amstad, E.; Schmid, T.; Stadler, J.; Zenobi, R. Nanoscale probing of a polymer-blend thin film with tip-enhanced Raman spectroscopy. *Small* **2009**, *5*, 952–960.
25 Dunn, R. C. Near-field scanning optical microscopy. *Chem. Rev.* **1999**, *99*, 2891–2927.
26 Hecht, B.; Sick, B.; Wild, U. P.; Deckert, V.; Zenobi, R.; Martin, O. J. F.; Pohl, D. W. Scanning near-field optical microscopy with aperture probes: fundamentals and applications. *J. Chem. Phys.* **2000**, *112*, 7761–7774.
27 Nabha-Barnea, S.; Maman, N.; Visoly-Fisher, I.; Shikler, R. Microscopic investigation of degradation processes in a polyfluorene blend by near-field scanning optical microscopy. *Macromolecules* **2016**, *49*, 6439–6444.
28 Creton, C. Molecular stitches for enhanced recycling of packaging. *Science* **2017**, *355*, 797–798.
29 Garcia, J. M.; Robertson, M. L. The future of plastics recycling. *Science* **2017**, *358*, 870–872.
30 Debolt, M. A.; Robertson, R. E. Morphology of compatibilized ternary blends of polypropylene, nylon 66, and polystyrene. *Polym. Eng. Sci.* **2006**, *46*, 385–398.
31 Cappella, B.; Kaliappan, S. K. Determination of thermomechanical properties of a model polymer blend. *Macromolecules* **2006**, *39*, 9243–9252.
32 Wang, D.; Fujinami, S.; Liu, H.; Nakajima, K.; Nishi, T. Investigation of reactive polymer-polymer interface using nanomechanical mapping. *Macromolecules* **2010**, *43*, 5521–5523.
33 Qu, M.; Deng, F.; Kalkhoran, S. M.; Gouldstone, A.; Robisson, A.; van Vliet, K. J. Nanoscale visualization and multiscale mechanical implications of bound rubber interphases in rubber-carbon black

nanocomposites. *Soft Matter* **2011**, *7*, 1066–1077.
34 Brune, P. F.; Blackman, G. S.; Diehl, T.; Meth, J. S.; Brill, D.; Tao, Y.; Thornton, J. Direct measurement of rubber interphase stiffness. *Macromolecules* **2016**, *49*, 4909–4922.
35 Zhang, M.; Li, Y.; Kolluru, P. V.; Catherine Brinson, L. Determination of mechanical properties of polymer interphase using combined atomic force microscope (AFM) experiments and finite element simulations. *Macromolecules* **2018**, *51*, 8229–8240.
36 Wang, D.; Russell, T. P.; Nishi, T.; Nakajima, K. Atomic force microscopy nanomechanics visualizes molecular diffusion and microstructure at an interface. *ACS Macro Lett.* **2013**, *2*, 757–760.
37 Wang, D.; Nakajima, K.; Liu, F.; Shi, S.; Russell, T. P. Nanomechanical imaging of the diffusion of fullerene into conjugated polymer. *ACS Nano* **2017**, *11*, 8660–8667.
38 He, C. F.; Shi, S. W.; Wu, X. F.; Russell, T. P.; Wang, D. Atomic force microscopy nanomechanical mapping visualizes interfacial broadening between networks due to chemical exchange reactions. *J. Am. Chem. Soc.* **2018**, *140*, 6793–6796.
39 Dazzi, A.; Prater, C. B.; Hu, Q.; Chase, D. B.; Rabolt, J. F.; Marcott, C. AFM-IR: combining atomic force microscopy and infrared spectroscopy for nanoscale chemical characterization. *Appl. Spectrosc.* **2012**, *66*, 1365–1384.
40 Felts, J. R.; Cho, H.; Yu, M. F.; Bergman, L. A.; Vakakis, A. F.; King, W. P. Atomic force microscope infrared spectroscopy on 15 nm scale polymer nanostructures. *Rev. Sci. Instrum.* **2013**, *84*, 023709.
41 Dazzi, A.; Prater, C. B. AFM-IR: technology and applications in nanoscale infrared spectroscopy and chemical imaging. *Chem. Rev.* **2017**, *117*, 5146–5173.
42 Gong, L.; Chase, D. B.; Noda, I.; Liu, J.; Martin, D. C.; Ni, C.; Rabolt, J. F. Discovery of β-form crystal structure in electrospun poly[(*R*)-3-hydroxybutyrate-*co*-(*R*)-3-hydroxyhexanoate] (PHBHX) nanofibers: from fiber mats to single fibers. *Macromolecules* **2015**, *48*, 6197–6205.
43 Tang, F. G.; Bao, P.; Su, Z. H. Analysis of nanodomain composition in high-impact polypropylene by atomic force microscopy-infrared. *Anal. Chem.* **2016**, *88*, 4926–4930.
44 Wang, Z. Q.; Sun, B. L.; Lu, X. F.; Wang, C.; Su, Z. H. Copolymer distribution in core-shell rubber particles in high-impact polypropylene investigated by atomic force microscopy-infrared. *Macromolecules* **2020**, *53*, 2686–2693.
45 Rickard, M. A.; Meyers, G. F.; Habersberger, B. M.; Reinhardt, C. W.; Stanley, J. J. Nanoscale chemical imaging of a deuterium-labeled polyolefin copolymer in a polyolefin blend by atomic force microscopy-infrared spectroscopy. *Polymer* **2017**, *129*, 247–251.
46 Morsch, S.; Liu, Y. W.; Lyon, S. B.; Gibbon, S. R. Insights into epoxy network nanostructural heterogeneity using AFM-IR. *ACS Appl. Mater. Interfaces* **2016**, *8*, 959–966.
47 Kim, S. Y.; Khanal, D.; Kalionis, B.; Chrzanowshi, W. High-fidelity probing of the structure and heterogeneity of extracellular vesicles by resonance-enhanced atomic force microscopy infrared spectroscopy. *Nat. Protoc.* **2019**, *14*, 576–593.
48 Tai, T.; Karacsony, O.; Bocharova, V.; van Berkel, G. J.; Kertesz, V. Topographical and chemical imaging of a phase separated polymer using a combined atomic force microscopy/infrared spectroscopy/mass spectrometry platform. *Anal. Chem.* **2016**, *88*, 2864–2870.
49 Kenkel, S.; Mittal, A.; Mittal, S.; Bhargava, R. Probe-sample interaction-independent atomic force microscopy-infrared spectroscopy: toward robust nanoscale compositional mapping. *Anal. Chem.* **2018**, *90*, 8845–8855.
50 Felts, J. R.; Kjoller, K.; Lo, M.; Prater, C. B.; King, W. P. Nanometer-scale infrared spectroscopy of heterogeneous polymer nanostructures fabricated by tip-based nanofabrication. *ACS Nano* **2012**, *6*, 8015–8021.
51 Cartier, H.; Hu, G. H. Styrene-assisted free radical grafting of glycidyl methacrylate onto polyethylene in the melt. *J. Polym. Sci., Part A: Polym. Chem.* **1998**, *36*, 2763–2774.
52 Koning, C.; Van Duin, M.; Pagnoulle, C.; Jerome, R. Strategies for compatibilization of polymer blends. *Prog. Polym. Sci.* **1998**, *23*, 707–757.
53 Ajji, A.; Utracki, L. A. Interphase and compatibilization of polymer blends. *Polym. Eng. Sci.* **1996**, *36*, 1574–1585.
54 Li, H.; Chiba, T.; Higashida, N.; Yang, Y.; Inoue, T. Polymer-polymer interface in polypropylene/polyamide blends by reactive processing. *Polymer* **1997**, *38*, 3921–3925.
55 Yin, Z.; Koulic, C.; Pagnoulle, C.; Jerome, R. Probing of the reaction progress at a PMMA/PS interface by using anthracene-labeled reactive PS chains. *Langmuir* **2003**, *19*, 453–457.
56 Jeon, H. K.; Macosko, C. W.; Moon, B. J.; Hoye, T. R.; Yin, Z. H. Coupling reactions of end- *vs* mid-functional polymers. *Macromolecules* **2004**, *37*, 2563–2571.
57 Roeder, J.; Oliveira, R. V. B.; Goncalves, M. C.; Soldi, V.; Pires, A. T. N. Polypropylene/polyamide-6 blends: influence of compatibilizing agent on interface domains. *Polym. Test.* **2002**, *21*, 815–821.
58 Vermeesch, I. M.; Groeninckx, G.; Coleman, M. M. Poly(styrene-*co*-*n*-maleimide) copolymers: preparation by reactive extrusion, molecular characterization by FTIR, and use in blends. *Macromolecules* **1993**, *26*, 6643–6649.

https://doi.org/10.1007/s10118-021-2567-2